ISSN: 0975-8585

Research Journal of Pharmaceutical, Biological and Chemical Sciences

Wavelet Based Hybrid Compression and Color Clustering Segmentation Algorithm on CT/PET Images for Telemedicine Applications.

Pramod S*, and Ashish Payal

University School of Information, Communication and Technology, Guru Gobind Singh Indraprastha University, New Delhi, India.

ABSTRACT

Image compression plays a vital role in telemedicine for the data transfer. Out of the lossy and lossless compression algorithms, lossless technique is mostly preferred for medical images since there will be no loss of information. The CT/PET imaging is an efficient medical imaging modality for the analysis of tumors and the input data sets were preprocessed by median filter. The preprocessed images are compressed by hybrid technique comprising of discrete wavelet transform, run length coding and Huffman coding. The efficiency of the compression algorithm was analyzed by performance metrics like PSNR, MSE and compression ratio. The compressed images are retrieved in the receiver side by the decompression algorithm and the segmentation was done by color clustering binary tree quantization algorithm.

Keywords: Segmentation; clustering; median filter; Eigen vector.

Corresponding author

ISSN: 0975-8585

INTRODUCTION

Medical imaging modalities such as CT, MRI and PET made a radical change in the diagnosis of diseases in field of medicine. The Computer Tomography (CT), Magnetic Resonance (MR) and ultrasound modalities generate images for visualizing the anatomical structures. The Positron Emission Tomography (PET), Single Photon Emission Computed Tomography (SPECT) and functional magnetic resonance imaging are the functional imaging that provides information regarding metabolic functions of human body [1]. CT is the most commonly used cross sectional imaging technique to detect size and shape of tumor. PET scanning with Fluro De-oxy Glucose (18F-FDG) tracer is a non-invasive imaging method for assessment of glucose metabolism in the detection and classification of benign and malignant tumors [2]. The 3D nuclear activity maps derived from PET imaging is acquired from volumetric appropriation of positron emitting radio pharmaceuticals 18F-FDG after a specific time after injection. The accuracy of electron positron annihilation photons is measured for malignant tumor [3]. The cells which have higher metabolic activity on glucose at increased levels are due to the high energy demand which tends to be strong positive on PET [4]. The dual modality PET/CT scanner provides precise anatomical and functional images in a scanning session. Medical imaging role is inevitable in clinical diagnosis, treatment planning, surgical procedures and Picture Archiving and Communication Systems (PACS) which enables the storage and transfer of data [5]. Segmentation is the process of extraction of desired region of interest (ROI) and in case of medical images, ROI is a tumor or cyst. A wide variety of segmentation algorithms comprise of manual, semi-automatic and fully automatic, while the objective is to transmit the segmented image through the telemedicine network for the analysis by expert physicians [6].

Thomas Blaffert et al performed a near examination of threshold based and watershed segmentation algorithms on PET/MR images [7]. Nadia Withofs et al compared two automatic segmentation algorithms FLAB and GBM with two software products OASIS V1.8.3 (Segami Corporation, Columbia, (MD), EBW (Philips) for the tumor delineation (31 cases of rectal carcinoma). The FLAB algorithm based on statistical and fuzzy modelling was insensitive to noise and functions admirably on low spatial resolution images. The gradient based method (GBM) relies on watershed transform and cluster approach. The FLAB algorithm based on statistical and fuzzy modelling produces better results when compared to GBM [8]. Damon Wong et al proposed a region growing with knowledge based constraints method for semi-automated liver tumor segmentation with 10 training and 10 testing 2D slice datasets. The seed selection depends on manual labeling in the lesions which leads to sub optimal performance. [9].

Bing Nan Li et al proposed a unified level set model fused with gradient, prior information and region competition for the liver tumor segmentation on contrast enhanced CT images (25 two dimensional and 4 three dimensional images with 10 tumor datasets). The new level set model is robust to week boundaries and is very efficient to detect local objects at contrast enhanced CT images. [10]. Laurent Massoptier et al developed a fully automatic fast liver segmentation algorithm based on statistical model accompanied with active contour and gradient vector flow method which identifies the exact smooth boundaries. The statistical information is used to partition the images with rough boundaries which is adopted by adaptive histogram based thresholding technique [11].

Cherry Ballangan et al adopted a localized region based active contour segmentation model for tumor delineation (20 cases of lung tumor) and for avert the erosion of curve into normal liver pixel groups, the energy term used[12].

Compression algorithms are broadly classified into two categories lossy and lossless, however for medical images lossless technique is employed due to no loss of information in reconstruction. The compression ratio will not be much satisfactory in lossless approach, however many improved lossless techniques like modified Huffman, hybrid techniques and employing bio inspired optimization in conventional techniques are there in producing efficient results (13). Vinayak K Bairagi et al proposed a compression model in which ROI is compressed by lossless and non ROI is compressed by lossy technique which was developed for telemedicine applications. The ROI was compressed by Huffman, Arithmetic, RLE, LZW, ZIP, etc while the non ROI was compressed by integer wavelet with SPIHT algorithm [14]. Abdul KhaderJilaniSaudagar et al formulated a back propagation neural network based image compression to improve the quality of data transfer through the telemedicine network that produces better results than JPEG2000 standard (15). The paper organization is as follows. Materials and Methods comprises of data acquisition, algorithms description.

The MATLAB 2010a simulation results and evaluation of compression technique are presented in results and discussion and finally conclusions are drawn.

MATERIALS AND METHODS

Data acquisition

The image acquisition was done by HD Siemens PET/CT scanner. The eight data sets were taken into account in this paper and the standardized uptake value (SUV) indicates malignancy of liver tumor (Hepatic Cellular Carcinoma). The PET/CT scanner takes an average of 30 – 40 minutes to make complete body scan. The PET and CT images were acquired sequentially, in the same session. The PET and CT images were superimposed to a single image which has a slice thickness of 5mm by the inbuilt software in the HD Siemens PET/CT scanner. The compression and segmentation algorithms were tested on real time data sets and the results are portrayed in the results and discussion.

Preprocessing

Median filter replaces the center pixel value by the median value of gray level of all pixels of neighborhood. Median filter is a nonlinear spatial domain filter which preserves the edges and which do not cause blur effect when compared to other smoothing filters.
If I is the color image in RGB color space, then

$$I(x,y) = \begin{pmatrix} I_R(x,y) \\ I_G(x,y) \\ I_B(x,y) \end{pmatrix}$$

In this (x, y) is the location and I(x, y) is the pixel vector.

Each component of color image subjected to median filter are as follows

$$I[X_R, Y_R] = med_R \left\{ \frac{I(x,y)}{x,y \varepsilon w} \right\}$$
$$I[X_G, Y_G] = med_G \left\{ \frac{I(x,y)}{x,y \varepsilon w} \right\}$$
$$I[X_B, Y_B] = med_B \left\{ \frac{I(x,y)}{x,y \varepsilon w} \right\}$$

Where w is a window of odd size $I(X_B, Y_B)$ represents the coordinates of the median values for each color component.

A median vector m is formed by combining three vectors.

$$M = [I(X_R, Y_R), I(X_G, Y_G), I(X_B, Y_B)]$$

Compression and Decompression of medical images

The proposed system block diagram is shown in figure 1. The hybrid compression technique comprising of discrete wavelet Transform (DWT), Run length coding and Huffman coding is employed in this paper. In image processing, the operation can be performed in spatial domain or transform domain. In spatial domain the operation is performed directly on pixel, while the transforms domain operation deals with frequency. Many mathematical transforms are there which are having immense application in image processing like pre-processing, segmentation, compression and pattern recognition. The multiresolution property of wavelet transform makes it superior for many applications than other transforms like Discrete Fourier Transform (DFT) and Fast Fourier Transform (FFT).

The 2D DWT decomposes the input image into four sub bands and is depicted in figure 2.

ISSN: 0975-8585

- Approximate image component (LL)
- Horizontal detail components (HL)
- Vertical detail components (LH)
- Diagonal detail components (HH)

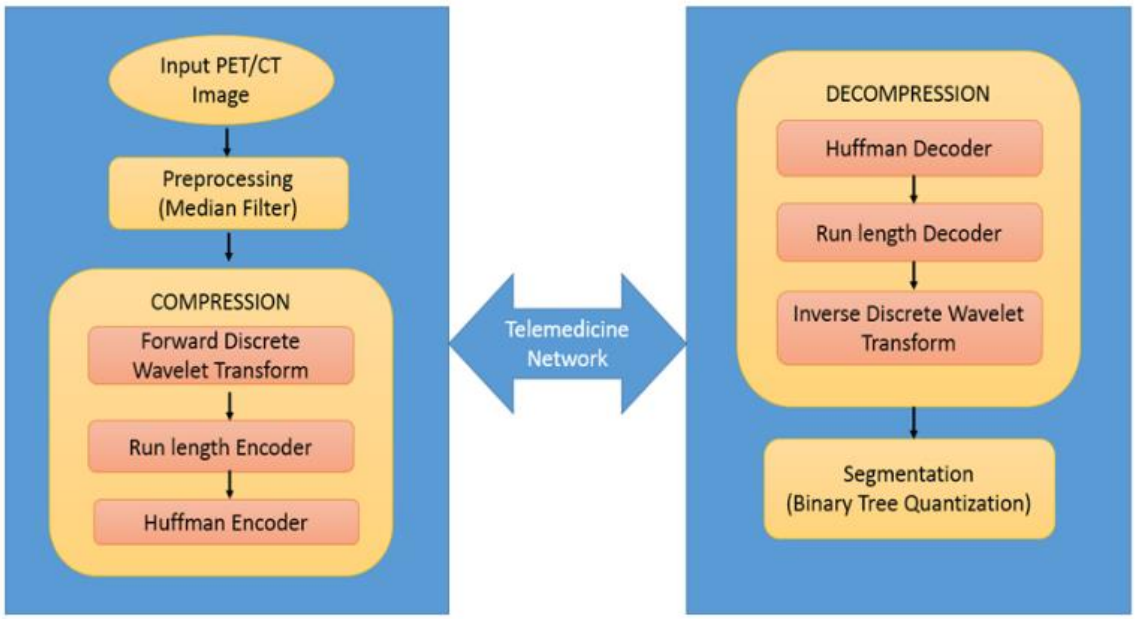

Figure 1: Block diagram of the proposed system

Removal of background

After the removal of optical disk, the median filter was applied for the removal of noise generated in the previous stage. The morphological open operation was then performed on the median filter output and it is subtracted from the median filter output for the removal of background. Fig 3 shows the removal of background by using morphological opening operation.

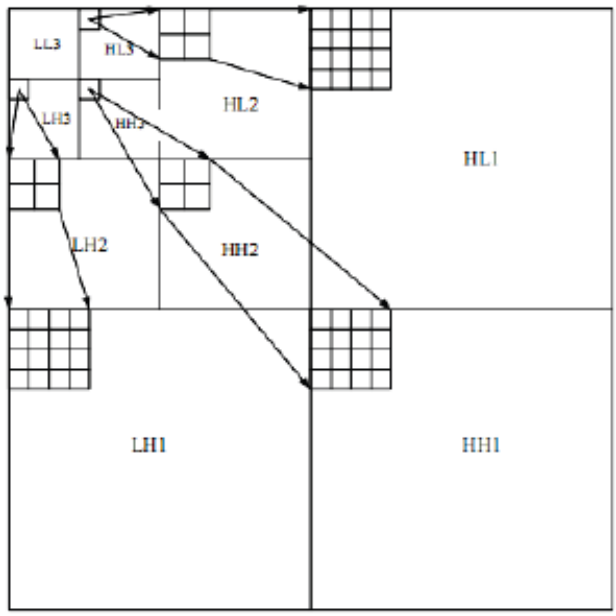

Figure 2: Three level wavelet decomposition

The most of the signal energy is concentrated in the approximate sub band, hence image compression in this band provides high compression ratio. Depending upon the decomposition level (N), each time the LL sub band is splitted into four components LL, HL, HH, and LH. The three level DWT decomposition of the image is depicted in figure 2. After the wavelet decomposition, quantization and thresholding of coefficients are done. During this process, the relationship between parent and children of wavelet structure is exploited. In quantization, all the coefficients are divided by quantization step and round of them to nearest integer. The quantization step differs for each sub band in accordance with the range of values and hard thresholding is employed for each sub band. The parent coefficient and its four children are considered to be zero, when its value is lower than the threshold value. In the encoding section, forward wavelet transform is applied and in the decoding section, the inverse transform is applied.

The Huffman coding and run length coding are lossless compression techniques and are employed in this paper after decomposition by wavelet transform. The quantization and thresholding introduce many zero in the sub band. The coefficients are encoded using run length encoding (RLE) except the LL3 sub-band, since it does not have much long run of zeros. The redundant run length coded coefficients are subjected to Huffman coding and are converted into bit stream. The compressed image is in the form of bit stream and is in non-visual format. The compressed image can be transmitted for communication purpose. The decompression is the inverse process of compression as indicated in the figure 1. In the decompression process, the reconstructed image gives satisfactory quality and was evaluated by performance metrics like PSNR and compression ratio.

Binary Tree Quantization Algorithm

The binary tree quantization is a color clustering technique. The image is a two dimensional array of 'N' pixels and the set of all grid points is denoted by P. The members $p \epsilon P$ may be written as $p(i,j)$ where i indicates the row index and j indicates the column index. The input image and the intensity value of the pixel at grid point 'p' is denoted as $x_p = (r_p, g_p, b_p)^t$. The r_p , g_p , b_p are the red, green and blue colour component for the pixel. The objective of the binary tree quantization algorithm is to partition 'P' into 'C' disjoint sets or clusters. The Partition is in the form of binary tree structure and each node represents the subset of P, the child nodes of any node partition are the member of corresponding parent nodes.

Let C_n represents image pixels for node to node 'n'. The root node is labelled as 1 and the children of the n^{th} node is labelled as 2n and 2n+1. The pixel in P are coded in such a manner that each leaf node with a single colour in the palette is comprised of all the pixels. The leaf node sets are stored as linked list and upon the splitting of a node, it is reorganized into two list. The constraints for the formation of binary tree is indicated by number of leaves C and the method of splitting the node into two children.

The total squared difference (TSD) between the actual and quantized image is a criteria that determines which node to split and its value should be minimized. TSD is defined as follows

$$TSD = \sum_{\substack{all\ leaves \\ n}} \sum_{p \epsilon C_n} \| x_p - q_n \|^2$$

Where, q_n is the quantization value and C_n is the color set.

The second order statistics based parameters is used to determine the order and the splitted nodes results in the creation of binary tree. The following are the cluster statistics used in the formation of binary tree.

$$R_n = \sum_{p \epsilon C_n} x_p x_p^T$$

Where R_n represents the variance and it is a 3x3 matrix.

$$m_n = \sum_{p \epsilon C_n} x_p$$

Where m_n represents the mean and it is a 3 component vector.

$$N_n = |C_n|$$

ISSN: 0975-8585

Where $N_n$represents the total number of clusters.

Assume that the quantization value of a cluster q_n should be equal to the cluster mean.

$$q_n = \frac{m_n}{N_n}$$

The node having quantization level q_n is splitted into two nodes and having new quantization level q_{2n} andq_{2n+1}. Each cluster member is associated with any one of the two nodes with closer quantization level. More precisely, it is equivalent to select a plane that best splits the cluster color. In general, we can obtain the unit vector *e* which maximizes the expression.

$$\sum_{p \epsilon C_n} \left((x_p - q_n)^T \right)^2 = e^T \hat{R}_n e$$

The $\hat{R}_n$ is the cluster covariance and can be written as

$$\hat{R}_n = R_n - \frac{1}{N_n} m_n m_n^T$$

The solution of the above equation is Eigen vectore_n that corresponds to the largest or principal Eigen vector $\lambda_n$of $\hat{R}$. The total squared variation in the direction of e_n can be written as follows

$$\sum_{p \epsilon C_n} \left((x_p - q_n)^T \right)^2 = \lambda_n$$

The cluster C_n can be splitted into two sets $C_{2n}$and $C_{2n+1}$are depicted in the figure 3 below.

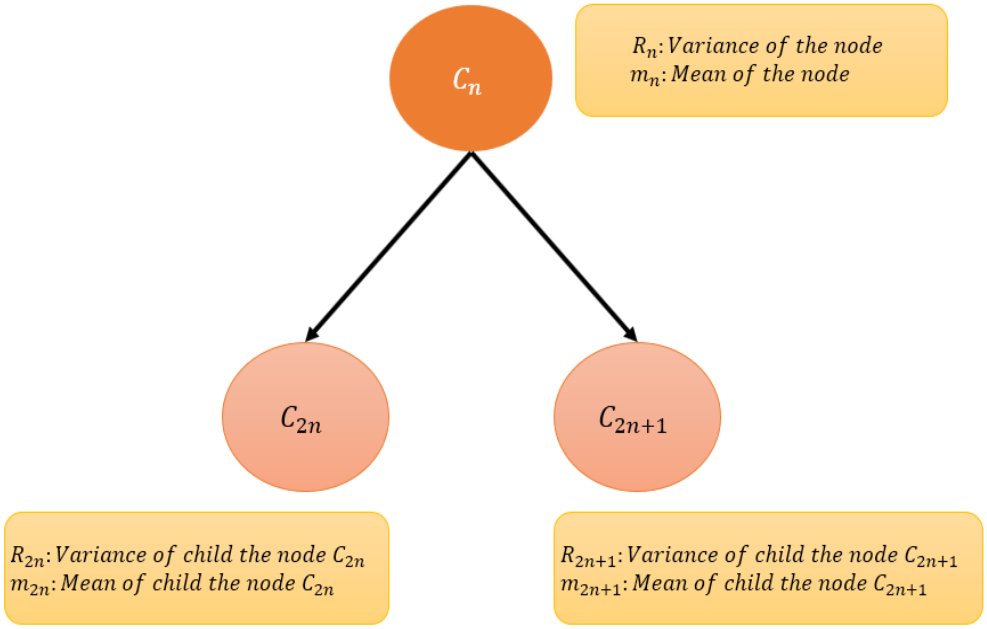

Figure 3: Node splitting in color clustering algorithm

Where,

$$C_{2n} = \{p \epsilon C_n : e_n^T x_p \leq e_n^T q_n\}$$
$$C_{2n+1} = \{p \epsilon C_n : e_n^T x_p > e_n^T q_n\}$$
$$R_{2n+1} = R_n - R_{2n}$$
$$m_{2n+1} = m_n - m_{2n}$$
$$N_{2n+1} = N_n - N_{2n}$$

ISSN: 0975-8585

The objective of splitting the node is based on the minimized value of TSD. When a node is splitted into sub nodes, the variance of the node is reduced based on the direction of principal Eigen vector.

RESULTS AND DISCUSSION

The proposed algorithm was executed in MATLAB 2013a on 2.6 GHz Intel core i5 processor with 4GB RAM and 64bit Windows 10 operating system. The expert physician selects the region of interest (ROI) in CT/PET image manually in order to determine the SUV value. The algorithms were evaluated on 8 datasets, each comprising of 60 slices .The results of the typical slices from dataset 1, 4 and 8 are depicted here. The preprocessing was done by median filter, before the compression is done. The malignancy stage of tumor is determined by the SUV value which ranges between 6<SUVmax<40. The higher value of SUV indicates the aggressive nature of the malignant tumor. The input PET/CT image from the datasets are depicted in figure 4.

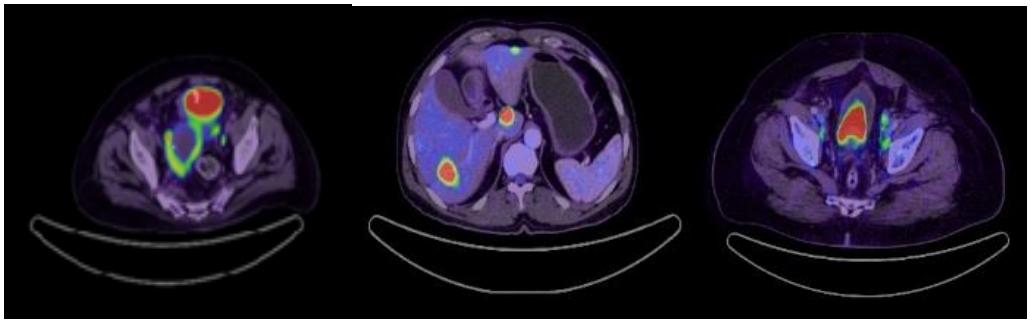

(a) (b) (c)

Figure 4: Input PET/CT image from data set 1, 4, 8

The primary components R, G and B were extracted from the input CT/ PET image. The primary components R, G and B were preprocessed using median filter of 3×3 window size. The red, green and blue denoised component of median filter corresponding to the input image is depicted in figure 5.

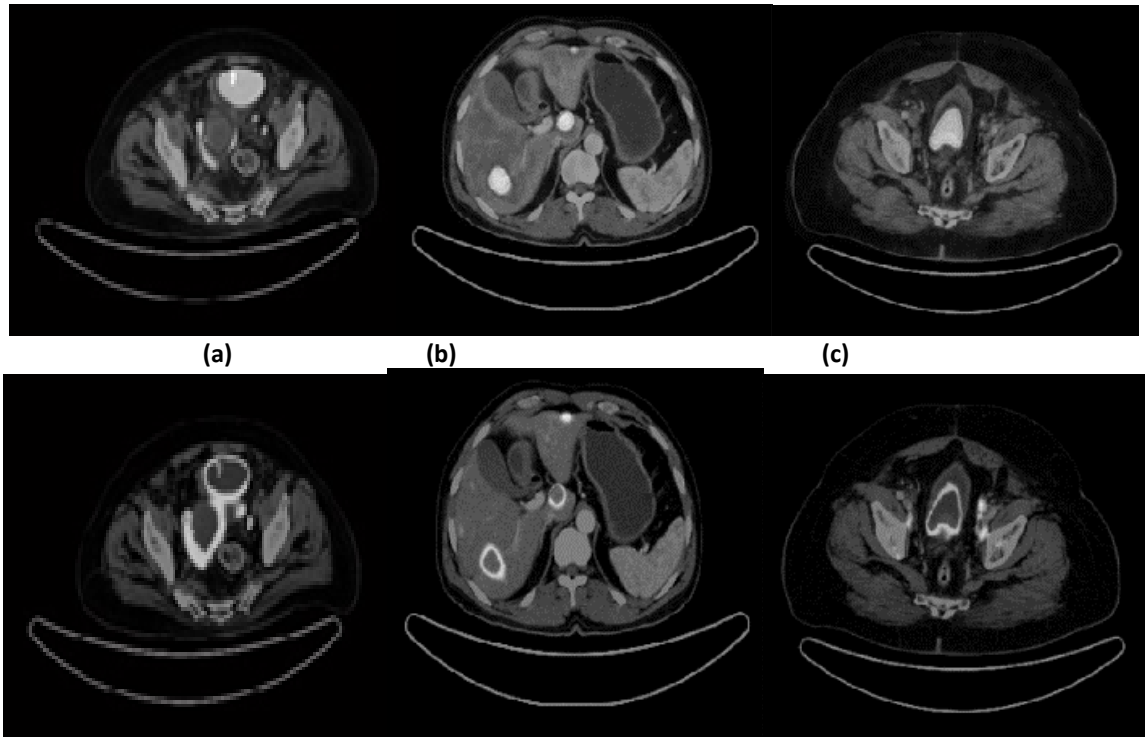

(a) (b) (c)

(d) (e) (f)

ISSN: 0975-8585

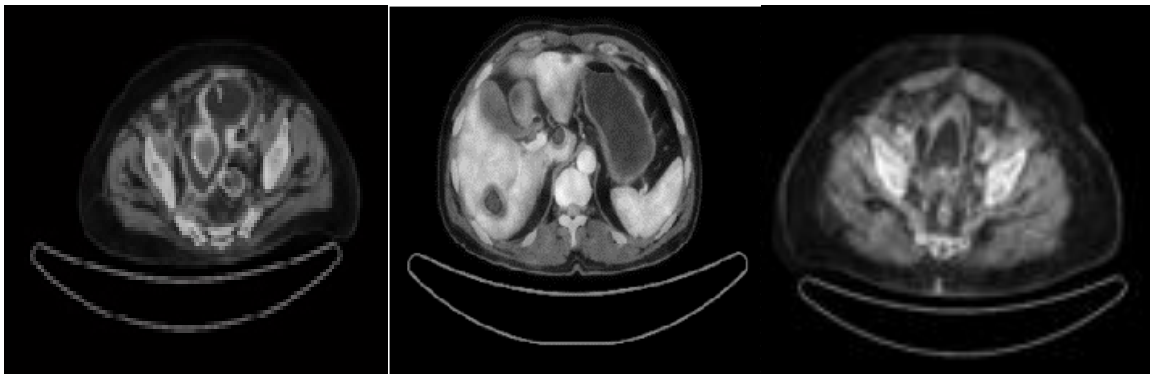

(g) (h) (i)

Figure 5: (a,d,g) R component denoised, (b,c,h) G component denoised, (c,f,i) B component denoised

The figure 6 depicts the denoised image after median filtering. The preprocessed output image from the median filter was subjected to hybrid compression algorithm. The compression of the medical images was done by a hybrid approach comprising of wavelet transform, run length coding and Huffman coding.

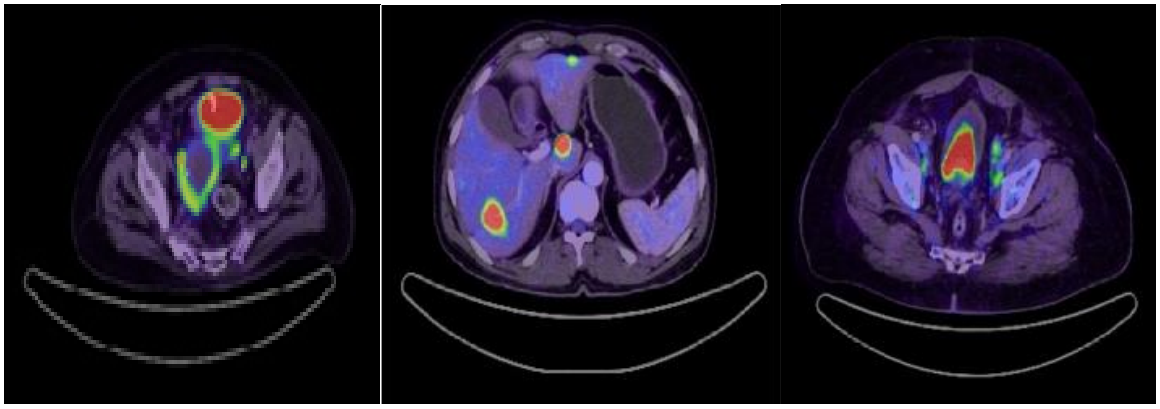

(a) (b) (c)

Figure 6: Median filter output

The hybrid compression algorithm produces better results when compared with the wavelet approach and hybrid approach comprising of wavelet transform and run length coding. In the encoding section, the forward transform is employed and in the decoding section, the reverse transform is employed. The proposed compression algorithm was evaluated by the performance metrics like PSNR, MSE.

$$PSNR = 10log_{10}\left(\frac{255 * 255}{MSE}\right)$$

$$MSE = \frac{1}{MN}\sum_{i=0}^{M-1}\sum_{j=0}^{N-1}[X(i,j) - Y(i,j)]^2$$

ISSN: 0975-8585

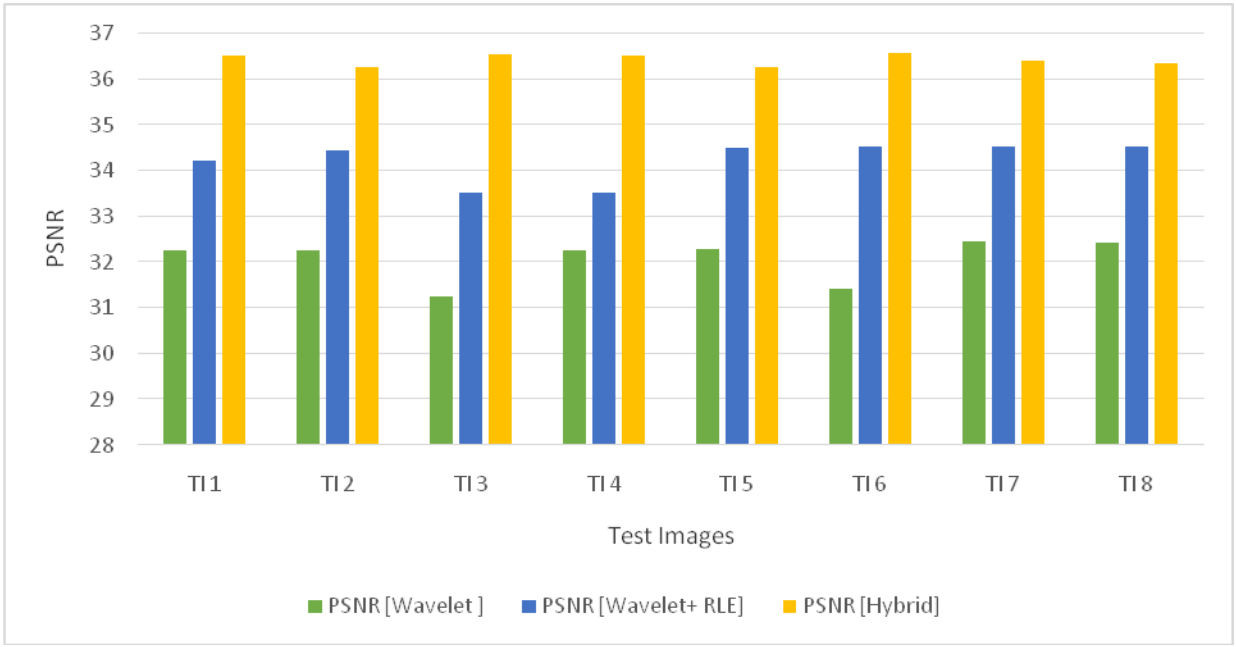

Figure 7: PSNR plot of compression techniques

The PSNR plot in figure 7 shows that, the hybrid compression approach (Wavelet + Run length coding + Huffman coding approach) is better than the other two approaches (Wavelet transform, Wavelet transform and Run length approach). The MSE plot in figure 8 also shows the proficiency of the compression algorithm. Here TI 1 to TI 8 represents the typical slice from each dataset.

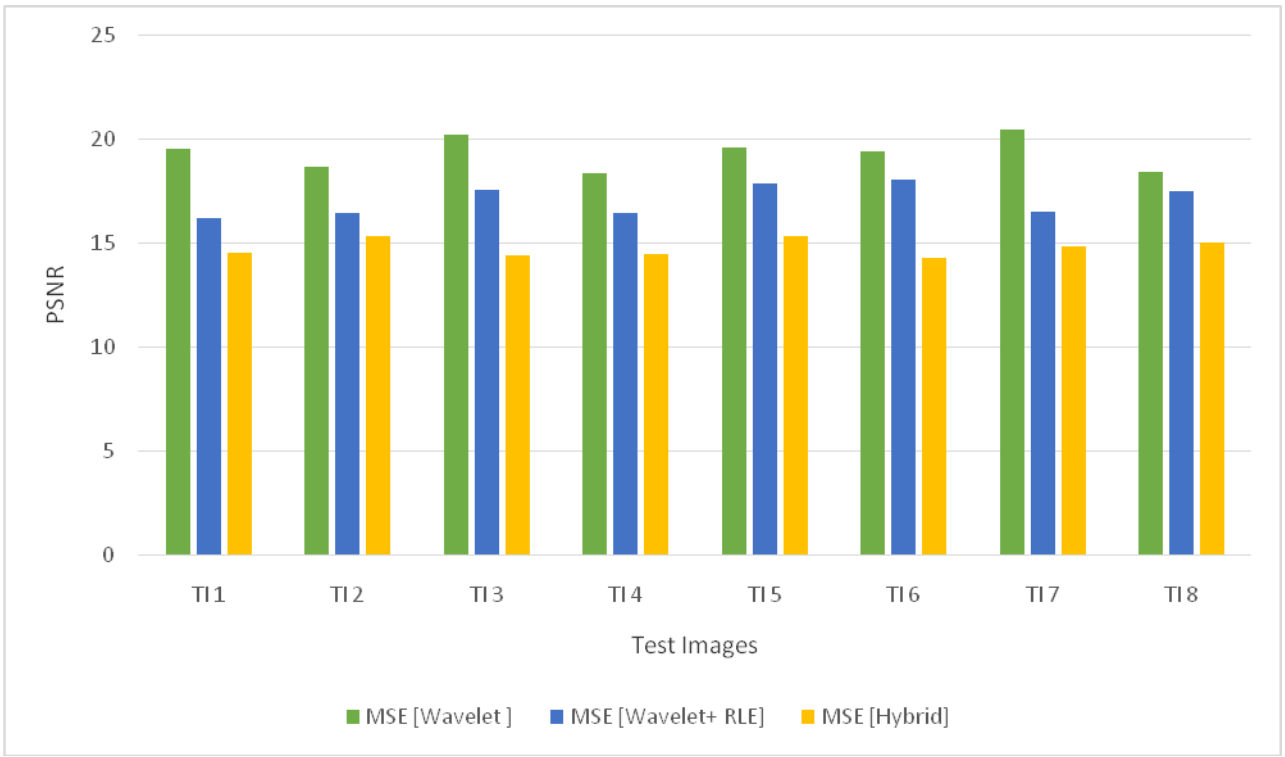

Figure 8: MSE plot of compression techniques

ISSN: 0975-8585

The compression ratio is also an efficient metric for the evaluation of compression technique and can be written as follows

$$CP = 100 \times \left(1 - \frac{I_c}{I}\right)$$

Where I_c is Compressed Image size and I is the Original image size. The compression ratio in percentage is depicted below in table 1.

Table 1: Compression ratio for different test images.

Test Image	Size of Test Image	Compression Percentage
TI 1	512x512	68.75
TI 2	512x512	73.58
TI 3	512x512	75.55
TI 4	512x512	76.00
TI 5	512x512	69.76
TI 6	512x512	75.00
TI 7	512x512	68.18
TI 8	512x512	77.77

In the decoding section, the decompression is done and the reconstruction of the image takes place. The extraction of ROI was done by color clustering algorithm. The binary tree quantization color clustering algorithm generates the cluster outputs iteratively, shown in figure 7. The tumor region is segmented precisely with its shape and size. In the proposed binary tree quantization algorithm the cluster selection is done optimally as C=4 for all the input datasets.

The segmentation result of the decompressed medical images corresponding to the images in figure 6 are depicted below. For the typical slice in data set1, clustering result C=2 is valid for tumor analysis. Similarly for the typical slice in data set 4 and 8, clustering result C=1 and C=4 provides valid result in tumor segmentation.

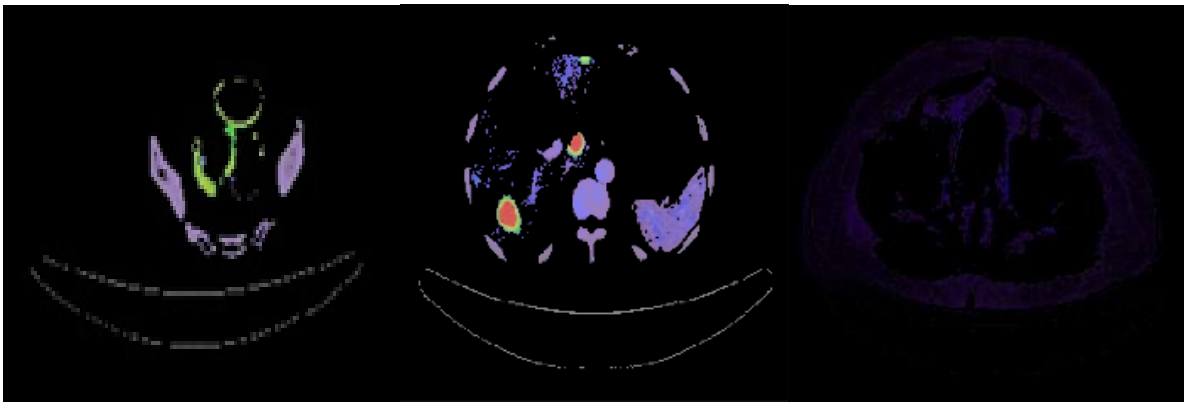

(a) **(b)** **(c)**

ISSN: 0975-8585

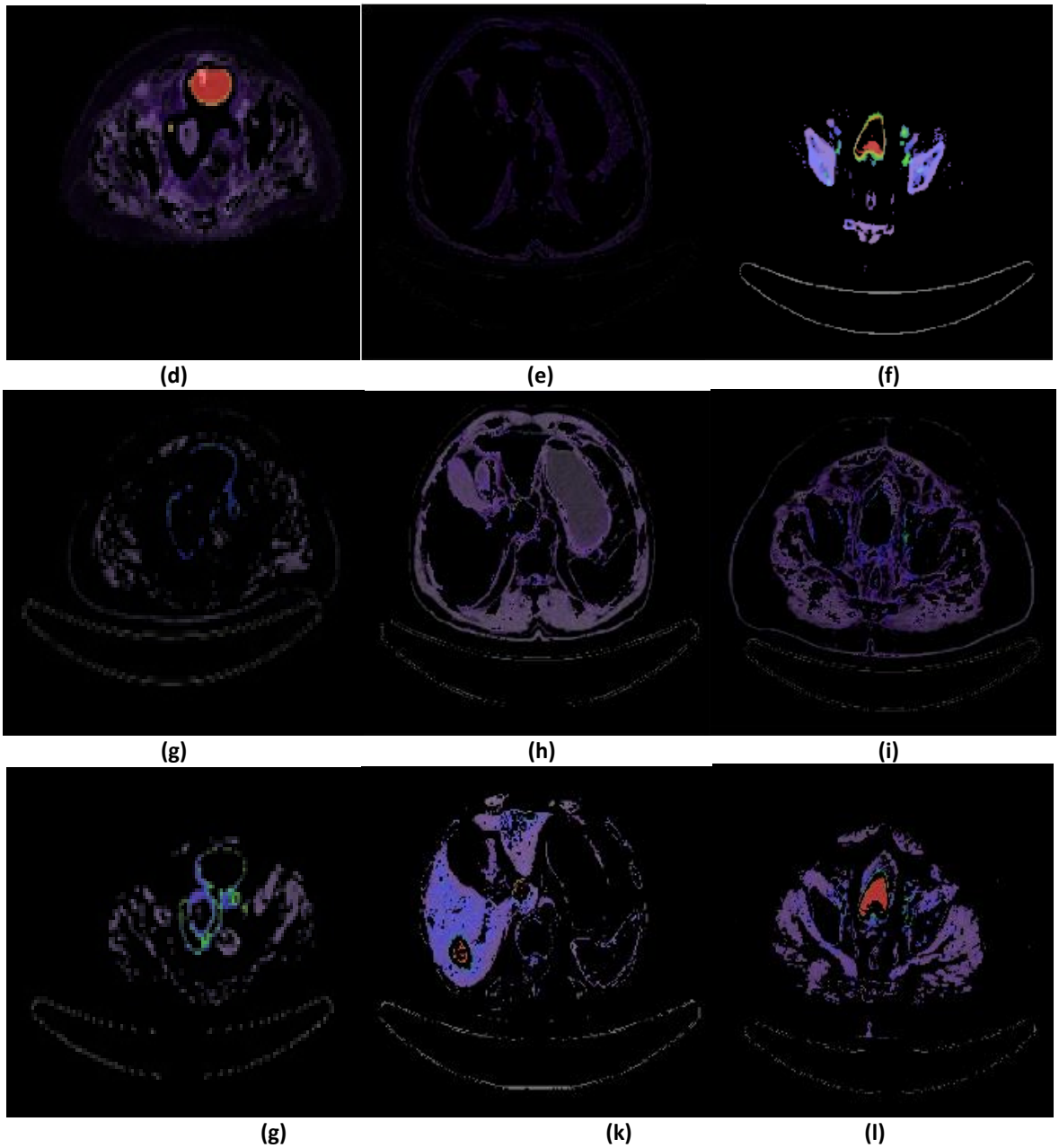

Figure 9: (a, b, c, d) Cluster output of binary tree quantization algorithm from the typical slice from the data set 1, 4, 8 with C=4

CONCLUSION

This paper proposes a lossless compression and segmentation algorithm for telemedicine algorithms. The preprocessing of the datasets was done by a hybrid technique comprising of Wavelet Transform, Run Length Coding and Huffman Coding. The Huffman Coding algorithm was evaluated by performance metrics like PSNR, MSE and Compression Percentage and it produce good results. The segmentation was done by binary tree quantization color clustering algorithm effectively delineate the tumor region. The compressed images can be transmitted from rural Health Centre to super specialty hospitals through the telemedicine network.

REFERENCES

[1] Michael J. R, Holgerstrunk, T G, Roland R, Ursula J, Jan B, Tilman S, Hans-J B and Franz L. D. 2005. Detection of Klatskin's Tumor in Extrahepatic Bile Duct Strictures using Delayed 18F-FDG PET/CT:

Preliminary Results for 22 patient Studies. *The journal of nuclear medicine*. 46, 7, (July 2005), 1158-1163.

[2] Soma K, Yukiko A, Azusa T, Tetsuya H, Takahito N and Yoshito T. 2014. A Case of multiple hepatic angiomyolipomas with high 18 F-flurodeoxy glucose uptake. *Bio medical central imaging*. 14, 17, (May 2014).

[3] S.D.Wollenweber, Ambwani S, A.H.R. Lonn, D. Shanbhag, S.Thiruvenkadam. 2013. Comparsion of 4-Class and Continuous Fat/Water Methods for Whole-Body, MR-Based PET Attenuation Correction. *IEEE transaction on nuclear science.* 60, 5, (Oct 2013), 3391 – 3398.

[4] Shuo J, Dengwang L, Hongjun W, Yong Y. 2013. Registration of PET and CT images based on multiresolution gradient of mutual information demons algorithm for positioning esophageal cancer patients. Journal of Applied Clinical Medical Medicinal Physics. 14, 1, (Jan 2013), 3931.

[5] Ingrid S, Til A, Thomas M. D. and Torsten K. 2011. Challenges of medical image processing. ComputSci Res Dev. 26, 1 (Nov. 1993), 5-13.

[6] Divya M and Janet J. 2011. Design and Implementation of a Hybrid Compression Technique for Ultrasound Images in Telemedicine. 2, 7, 111-130.

[7] Thomas B, Steffen R, Jing T, Manoj N and Zhiqiang H. Comparsion of threshold-based and watershed-based segmentation for the truncation compensation of PET/MR images. Proc. SPIE 8314, Medical Imaging 2012: Image Processing, 831403 (14 February 2012);

[8] Nadia W, Claire B, Catherine van der R, Philippe M, Mathieu H, Sebastien J, Dimitris V, John, A. L, Philippe A. C and Roland H, 2014. FDG PET/CT for rectal carcinoma radiotherapy treatment planning: comparison of functional volume delineation algorithms and clinical challenges. Journal of applied clinical medical physics. 15, 5, (Sep 2014).

[9] Damon W, Jiang L, Yin F. 2008. A semi-automated method for liver tumor segmentation based on 2D region growing with knowledge-based constraints. The MIDAS Journal, 2008.

[10] Bing N L, Chee KC, Stephen C, Sim H O. 2012. A new unified level set method for semi-automatic liver tumor segmentation on contrast-enhanced CT images. Expert Systems with Applications, 39, 2012, 9661–9668.

[11] Laurent M, Sergio C. 2008. A new fully automatic and robust algorithm for fast segmentation of liver tissue and tumors from CT scans. EurRadiol, 18, 8. (Aug 2008). 1658–1665.

[12] Cherry B, Xiuying and Dagan F. 2011. Lung Tumor Delineation in PET-CT Images Based on a New Segmentation Energy. IEEE Nuclear Science Symposium Conference Record, (Oct 2011), 3202 – 3205.

[13] Janet.J, Natesan T.R., 2005. Effective image compression technique for medical images in Telemedicine. Asian Journal of Information Technology, 4, 12, 1180-1186.

[14] Vinayak K B, and Ashok M S. 2013. ROI-based DICOM image compression for telemedicine. Digital Image Processing, Indian Academy of Sciences. 38, 1, (Feb 2013), 123–131.

[15] Abdul K J S and Omar A. S. 2014. Neural Network Based Image Compression Approach to Improve the Quality of Biomedical Image for Telemedicine. British Journal of Applied Science & Technology. 4, 3, (Oct 2013), 510-524.